Wang *et al. Energy Mater.* **2025**, *5*, 500056
DOI: 10.20517/energymater.2024.136

Energy Materials

Article

Open Access

Check for updates

Mesostructured Pt alloy nanotubes with synergistic edge sites as bifunctional electrocatalysts for direct ethanol fuel cells

Shensong Wang[1,#], Zhiliang Zhao[2,#], Yongming Hu[1,*], Sanping Jiang[2,3,*], Xinyi Zhang[1,2,*]

[1]Hubei Key Laboratory of Micro-Nanoelectronic Materials and Devices, School of Microelectronics, Hubei University, Wuhan 430062, Hubei, China.
[2]National Energy Key Laboratory for New Hydrogen-Ammonia Energy Technologies, Foshan Xianhu Laboratory, Foshan 528200, Guangdong, China.
[3]Minerals, Energy and Chemical Engineering, Western Australian School of Mines, Curtin University, Perth, WA 6845, Australia.
[#]Authors contributed equally.

***Correspondence to:** Prof. Yongming Hu, Hubei Key Laboratory of Micro-Nanoelectronic Materials and Devices, School of Microelectronics, Hubei University, No. 368 Youyi Avenue, Wuchang District, Wuhan 430062, Hubei, China. E-mail: Huym@hubu.edu.cn; Prof. Sanping Jiang, National Energy Key Laboratory for New Hydrogen-Ammonia Energy Technologies, Foshan Xianhu Laboratory, No. 1 Yangming Road, Nanhai District, Foshan 528200, Guangdong, China. E-mail: s.jiang@curtin.edu.au; Prof. Xinyi Zhang, Hubei Key Laboratory of Micro-Nanoelectronic Materials and Devices, School of Microelectronics, Hubei University, No. 368 Youyi Avenue, Wuchang District, Wuhan 430062, Hubei, China. E-mail: xinyizhang@hubu.edu.cn

How to cite this article: Wang, S.; Zhao, Z.; Hu, Y.; Jiang, S.; Zhang, X. Mesostructured Pt alloy nanotubes with synergistic edge sites as bifunctional electrocatalysts for direct ethanol fuel cells. *Energy Mater.* **2025**, *5*, 500056. https://dx.doi.org/10.20517/energymater.2024.136

Received: 25 Aug 2024 **First Decision:** 12 Nov 2024 **Revised:** 21 Nov 2024 **Accepted:** 9 Dec 2024 **Published:** 26 Feb 2025

Academic Editor: Ho Won Jang **Copy Editor:** Fangling Lan **Production Editor:** Fangling Lan

Abstract

Direct ethanol fuel cells are considered indispensable and prospective energy storage devices due to their high volumetric energy density. Platinum (Pt) and Pt-based alloys are regarded as the most effective catalysts for both oxygen reduction reaction (ORR) and ethanol oxidation reaction. To further enhance the catalytic performance of the catalyst, it is necessary to improve the mass activity and utilization efficiency of Pt. In this work, we report a strategy for fabricating ordered mesostructured platinum-palladium alloy nanotubes (MPPNs) with high hierarchical porosity (68%) and abundant exposed active edge sites. MPPNs exhibit excellent catalytic activity and stability for ORR, with a mass activity approximately 7.4 times higher than that of the commercial Pt/C catalyst. After 20 k cycles of accelerated durability test for ORR, MPPNs demonstrate impressive retention of their original mass activity, maintaining a value of 93.9%. Furthermore, they display superior catalytic activity and stability for ethanol oxidation reactions, with a mass activity about 2.4 times higher than that of commercial Pt/C. After the

2,000 scan cycles, the mass activity remains at 84.5% of initial performance. Both experimental and theoretical studies reveal that the synergistic effect of neighboring (111) and (100) facets on the edge sites plays a critical role in enhancing the electrocatalytic selectivity, activity and stability.

Keywords: Mesoporous PtPd nanotubes, ethanol oxidation reaction, oxygen reduction reaction, bifunctional electrocatalysts, edge sites

INTRODUCTION

Direct ethanol fuel cells (DEFCs) are regarded as a promising power candidate for electronic portable devices due to their high mass energy density (8.0 kWh/kg) and low environmental pollution[1-3]. However, their commercialization has been hindered by the high cost of noble catalysts and the sluggish kinetics of electrode reactions of existing electrocatalysts. The development of highly active catalysts for electrooxidation of ethanol molecules at the anode and reduction of oxygen at the cathode are urgent needs for the practical applications of DEFCs. The complete ethanol oxidation to CO_2 involves 12 electrons and a multi-step mechanism with the formation of poisoning intermediates. Among the intermediates, the CO_{ads} (adsorbed CO) is the main poisoning species for Pt-based catalysts, which not only decreases the energy capacity but also deactivates the anode reactions. On the other hand, the slow dynamics of oxygen reduction reaction (ORR) at the cathode and inefficient ethanol oxidation reaction (EOR) at the anode due to the chemically stable carbon-carbon (C-C) bond of ethanol are also key limiting factors impeding the widespread application of DEFCs[4,5]. Therefore, it is essential to develop efficient and stable catalysts for both ORR and EOR.

Among various catalysts, platinum (Pt) and Pt-based alloys are considered the most effective for both ORR and EOR[6-11]. Extensive efforts now focus on the manufacturing and engineering of Pt-based nanostructures to achieve high-activity and high-stability catalysts. However, the state-of-the-art Pt catalysts do not display satisfied activity and long-term stability due to their nanoparticles agglomerating or detaching from the carbon support and the inevitable poisoning by intermediate species during the electrocatalytic reaction[12,13]. Recently, many efforts have been made in the development of one-dimensional (1D) Pt-based catalysts for ORR and EOR[14-18]. However, solid 1D nanomaterials contain a substantial proportion of metal in the bulk *vs.* at the surface, resulting in a low surface-to-volume ratio, and hence low efficient utilization of metal. To optimize the performance and utilization efficiency of Pt-based catalysts, the fabrication of nanocatalysts with a high level of active surface atoms and high accessibility of matter molecules is critical for applications in DEFCs.

The design of Pt-based alloys with various compositions has shown great potential for improving the catalytic activity, which offers more attractive opportunities for increasing Pt utilization and improving the functionalities compared with the single-metal counterparts[19-23]. However, Pt is very scarce and expensive, and it is easily devitalized during the electrooxidation of alcohols due to CO adsorption. Incorporation of a second metal (such as Pd, Ru and Au) into Pt is an effective way to enhance its electrocatalytic performance and CO tolerance[24]. Pd is the most Pt-like metal, especially for EOR, but much more abundant than Pt. Pd and Pt have similar electrochemical properties, and have drawn special attention due to their negligible lattice mismatch and excellent miscibility[25], which facilitates the formation of platinum-palladium (PtPd) solid solutions. Bimetallic Pt and Pd nanomaterials with special morphology have shown outstanding electrocatalytic activity and durability in the ethanol oxidation and ORR reaction[26-28]. The presence of Pd involves a change in the electronic property of platinum, which can weaken the CO-Pt bond and improve catalytic activity, resulting in an enhancement of the overall reaction rate[29]. Mesostructured nanotubes are a

special type of 1D nanomaterials composed of nanoporous channels with mesopore walls. Such bimodal pore size distribution is anticipated to enable fast mass transfer and high electroactivity because of the extremely high surface-to-volume ratios in combination with excellent accessibility. Herein, we report the fabrication of highly ordered mesostructured PtPd alloy nanotubes (MPPNs) as bifunctional catalysts for both ORR and EOR. Benefiting from the extremely high surface-to-volume ratio and active surface area, MPPNs exhibit prominent electrocatalytic performance with high mass activity and stability and enhanced C-C dissociation kinetics and CO tolerance.

EXPERIMENTAL

Synthesis of MPPNs and nonporous PtPd nanowires

In a typical synthesis procedure, a gold film of about 10 nm thickness was deposited on one side of the anodic aluminum oxide (AAO) templates as electrodes by vacuum evaporation. The round-shaped AAO templates with diameters ~12 mm and thicknesses ~20 μm were filled with the prepared octaethylene glycol monohexadecyl ether ($C_{16}EO_8$) solution. The sample was sealed and maintained for 12 h at 65-80 °C to form a homogeneous $C_{16}EO_8$ solution within the nanochannels of the AAO template. The binary $C_{16}EO_8$-H_2O solutions containing 40-60 wt% $C_{16}EO_8$ were used for the formation of hexagonal lyotropic liquid-crystal (LLC) phases. The binary $C_{16}EO_8$-H_2O system is stable, and a homogeneous $C_{16}EO_8$ solution can be easily loaded into AAO at high temperatures. Then, the LLC-loaded AAO templates were cooled to room temperature (~25 °C) and immersed into the plating solution. Electrodeposition of PtPd alloy nanotubes was carried out from H_2PtCl_6 (12 wt%) and $PdCl_2$ (8 wt%) in 2 M HCl solution solutions by using a galvanostatic method at 100 μA cm^{-2}. After the deposition, the templates were etched away by using 1 M NaOH solution to release the mesoporous PtPd nanotubes. Nonporous PtPd nanowires (PPNWs) were also prepared under similar conditions without using $C_{16}EO_8$. All of the chemical reagents in this study were of analytical grade and supplied by Aladdin.

Materials characterization

Scanning electron microscopy (SEM, JEOL JSM-7100) and transmission electron microscopy (TEM, JEOL-2100F) were employed to investigate the morphology and structure of the mesoporous metal nanotubes. X-ray photoelectron spectroscopy (XPS) was performed using an ESCALAB 250 spectrometer (150 W, 1,486.6 eV). Nitrogen adsorption-desorption curves were measured using a specific surface area and porosity analyzer (ASAP 2020MC). Before measurement, the samples were degassed at 300 C for 5 h. In order to observe the cross sections of the MPPNs, the samples were mixed into Gatan G-1 epoxy (Mixing ratio of resin and hardener is 10:1). The mixtures were heated to form a fully cured flake. Then, the flake was polished to 30 μm by the Gatan polishing tool. Finally, sectioning was conducted on the Reichert-jung UltrCut S ultra-microtome by using a diamond knife from Diatome at room temperature. After sectioning, the microtome slices were floating on top of water bath and transferred onto copper grids for TEM analysis. The other slices were dissolved in butanone to remove the epoxy, and the MPPN samples were collected for electrochemical tests.

Electrochemical measurements

Electrochemical measurements were performed by means of electroanalytical instrument (autolab II) at room temperature. Pt and the KCl saturated Ag/AgCl electrode or a reversible hydrogen electrode (RHE) reference electrode were used as the counter and reference electrodes, respectively. The electrocatalytic performance of the obtained MPPNs with a diameter of 60 nm was investigated for the oxidation of ethanol and oxygen reduction. The catalysts were prepared by loading the synthesized samples with commercial carbon (Vulcan XC-72), and the mass loading was about 20 wt%. Then, 2.0 mg of catalyst was added to 2 mL aqueous solution containing 200 μL of 0.5 wt% Nafion solution (DuPont, USA) and 1.8 mL deionized (DI) water, and dispersed by sonication for 30 min. 20 μL of the catalytic suspension was loaded onto the

glassy carbon rotating disk electrode (RDE) by using a micropipette, yielding a PtPd loading of ~20.8 μg cm^{-2}. After the catalyst ink is dropped onto the RDE, the electrode is subsequently placed in a blast drying oven at 25 °C for 1 h to ensure thorough drying. Additionally, 3 mg of the commercial Pt/C catalyst (TKK, 46.7 wt% Pt) was dispersed in 2.0 mL 0.05 wt% Nafion solution and 10 μL of the mixture was pipetted onto the glassy carbon RDE, and the Pt loading is ~30.5 μg cm^{-2}. The CV curve recording was performed in an N_2-saturated 0.1 M $HClO_4$ solution. The ORR test was conducted in an O_2-saturated 0.1 M $HClO_4$ solution at a rotation rate of 1,600 rpm and normalized according to the geometric area of RDE (0.196 cm^2). The accelerated durability measurement was performed in an O_2- saturated 0.1 M $HClO_4$ ranging from 0.6 to 1.1 V *vs.* RHE at 100 mV s^{-1}. The EOR test was carried out in Ar-purged 0.1 M $HClO_4$ and 1.0 M CH_3CH_2OH solution at 50 mV s^{-1}. For CO-stripping test, the potential was kept at -0.14 V *vs.* Saturated Calomel Electrode (SCE) in a 0.1 M $HClO_4$ solution. Accelerated durability test (ADT) was carried out in an Ar-purged 0.1 M $HClO_4$ and 1.0 M CH_3CH_2OH solution at 100 mV s^{-1}. Finally, a chronoamperometry (CA) curve was recorded for 3,600 s with a sampling interval of 0.5 s.

Computational method

The density functional theory (DFT) calculations were performed on the software of Vienna Ab initio Simulation Package (VASP v.5.4.4) via projector augmented wave method. The correlation interactions and electron exchange were described by the Perdew-Burke-Ernzerhof and generalized gradient approximation[30,31]. The plane wave cutoff energy was set as 450 eV to realize high computational efficiency. PtPd(111), Pt(111)(200) and PtPd(111)(200) were modeled by means of the supercell approach with 4~6 layer atoms, and a 16 Å vacuum was applied in the *z*-direction. The convergence criteria of maximum energy and force were 1 × 10^{-5} eV and 0.03 eV $Å^{-1}$. The detailed calculation information is provided in Supplementary Material.

RESULTS AND DISCUSSION

Synthesis and characterization of MPPNs

MPPNs were produced by initially preparing hexagonal LLC mesophases within the AAO template, followed by the electrodeposition of the metals. A schematic of the preparation process is illustrated in Figure 1. Previous literature has reported that electrocatalysts with a Pt/Pd ratio of 3:1 present the best catalytic activity toward ORR and Anti-carbon monoxide poisoning properties during electrocatalytic oxidation of alcohols in acid solution[24,32,33]. Therefore, in this work, we have prepared the MPPN with a Pt/Pd ratio of 3:1 as the typical sample.

The XRD patterns of the MPPN powder are depicted in Figure 2A. The diffraction peak positions clearly correspond to the reflections of face-centered-cubic (FCC) PtPd alloy structure[34]. SEM images of the MPPN array, with diameters of approximately 60 nm, are shown in Figure 2B and C. The high-resolution SEM image reveals that the MPPNs consist of uniformly distributed mesopores, which are templated from the LLC mesophase. The energy-dispersive X-ray spectroscopy (EDS) analysis result reveals that the MPPNs mainly comprise Pt and Pd elements (with Cu originating from the substrate), with a Pt/Pd ratio of approximately 3/1, as shown in Figure 2D. The TEM images and their corresponding selected area electron diffraction (SAED) patterns of the MPPNs are presented in Figure 2E.

The SAED pattern confirms the FCC PtPd alloy structure, corroborating the XRD result. (inset of Figure 2E). Ordered mesopores are clearly visible on the surface of MPPNs. A high-magnification TEM image of MPPNs displays a highly ordered hexagonal arrangement of mesopores with a pore size of about 3 nm [Figure 2F]. Figure 2G and H, Supplementary Figure 1 exhibit the samples fabricated using a microtome. The MPPNs exhibit uniform morphology with a length of about 240 nm and maintain an

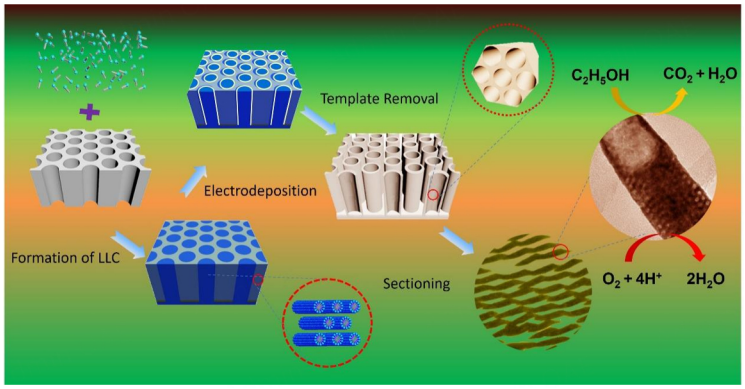

Figure 1. The schematic illustration of the fabrication process of MPPNs.

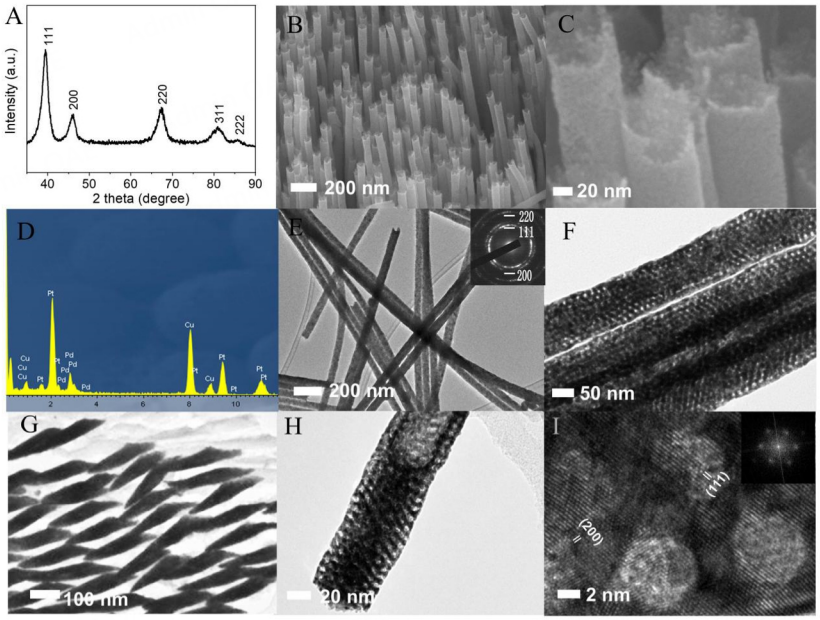

Figure 2. Material characterization of MPPNs. (A) XRD spectrum. (B and C) SEM images. (D) EDS spectroscopy. (E and F) TEM images and the corresponding electron diffraction pattern [inset in (E)]). (G and H) TEM images of the samples fabricated by microtome. (I) HRTEM image and the corresponding Fourier transform (FT) pattern (inset).

ordered mesoporous structure. Two obvious lattice spacings of 0.20 and 0.22 nm in the high-resolution TEM (HRTEM) image correspond to the (200) and (111) atomic planes of MPPNs, respectively [Figure 2I]. The corresponding Fourier transform images clearly reveal that the MPPN surface can be identified as the (110) planes of FCC PtPd solid solution alloy structure.

The surface elemental composition and chemical state of MPPNs were analyzed by X-Ray Photoelectron Spectroscopy (XPS). The XPS survey spectrum of the MPPNs is presented in Figure 3A. The surface atomic ratio of Pt/Pd is 74.4/25.6, consistent with the EDS result. The Pt 4f peaks located at 74.7 and 71.3 eV correspond to Pt Pt $4f_{5/2}$ and $4f_{7/2}$ of metallic Pt (0), respectively [Figure 3B][35]. The weaker doublets situated at 75.8 and 72.3 eV can be attributed to the surface Pt oxides[36]. Notably, Pt 4f binding energies of the MPPNs show a blue shift of 0.32 eV compared to those of Pt nanowires [Supplementary Figure 2]. The blue-shift of Pt 4f binding energies implies a higher electron density around the Pt atoms, leading to a

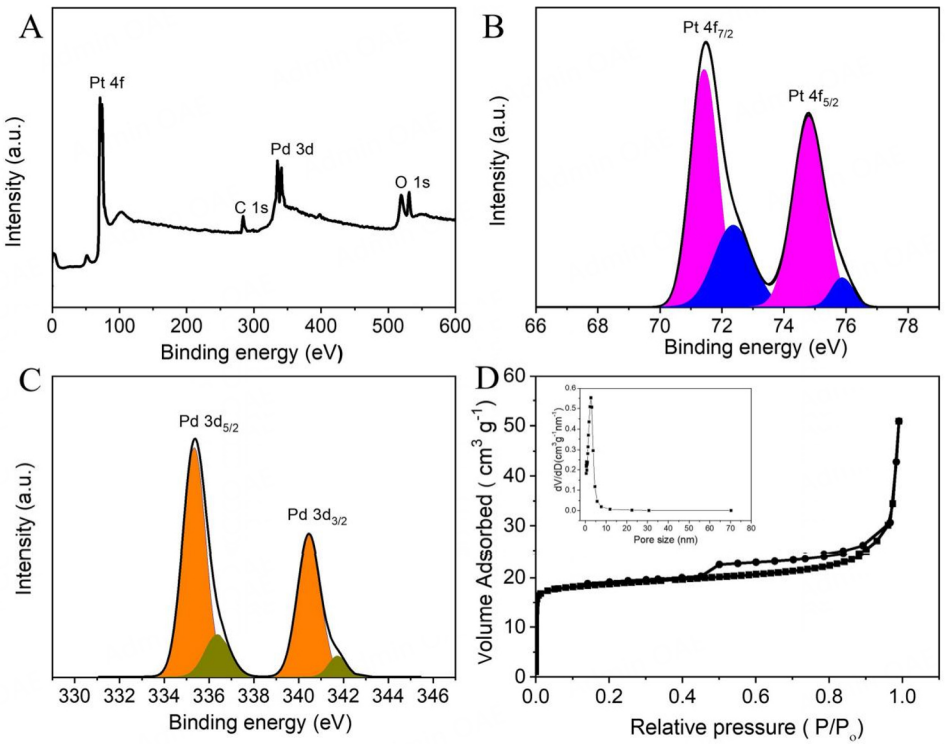

Figure 3. (A) XPS Survey spectrum, (B) Pt 4f, and (C) Pd 3d spectra of MPPNs. (D) N_2 sorption isotherm of MPPNs, and the corresponding pore size distribution (inset).

down-shift in the *d*-band center with respect to the Fermi level of the surface Pt atoms[37,38]. The change of the Pt *d*-band center can optimize the interaction between Pt and adsorption intermediates, thereby enhancing the catalytic activity of MPPNs. The Pd 3d spectrum is depicted in Figure 3C. The characteristic peaks of Pd $3d_{5/2}$ and Pd $3d_{3/2}$ of metallic Pd are located at 335.3 and 340.4 eV, respectively. The binding energy of the Pd 3d spectrum is blue-shifted compared to bulk Pd[39]. The two less intense peaks at 336.4 and 341.8 eV can be assigned to the oxidized state PdO[40]. The N_2 sorption isotherm of the MPPNs is depicted in Figure 3D. The Brunauer-Emmett-Teller (BET) surface area is about 45.4 $m^2 g^{-1}_{Pt+Pd}$. The pore size distribution curve [Figure 3D, inset] reveals that the MPPN samples exhibit a distinct mesoporous structure with a porosity of about 42.7% and an average pore size of 2.5 nm, respectively.

The electrocatalytic performance of MPPNs

The electrocatalytic performance of MPPNs was evaluated for ORR and EOR and compared with the nonporous PPNWs and commercial Pt/C catalysts. Figure 4A presents the cyclic voltammograms (CVs). The electrochemically active surface areas (ECSAs) were determined through the charges associated with the hydrogen adsorption zone and the loading of noble metal on the working electrode. The ECSAs of MPPNs, PPNWs and the commercial Pt/C catalysts are calculated to be 61.2, 48.9 and 52.3 $m^2 g^{-1}_{Pt+Pd}$, respectively.

The ORR polarization curves of the catalysts were collected from the rotating disc electrode in an O_2-saturated 0.1 M $HClO_4$ solution. As depicted in Figure 4B, the MPPNs exhibit a half-wave potential of 0.91 V, significantly higher than those of the PPNWs (0.89 V) and the commercial Pt/C (0.87 V), suggesting enhanced ORR activity of the MPPNs. Figure 4C illustrates the Tafel plots of MPPNs, PPNWs and the commercial Pt/C catalysts. The reduced Tafel slope of MPPNs (68 mV dec^{-1}), compared to the other

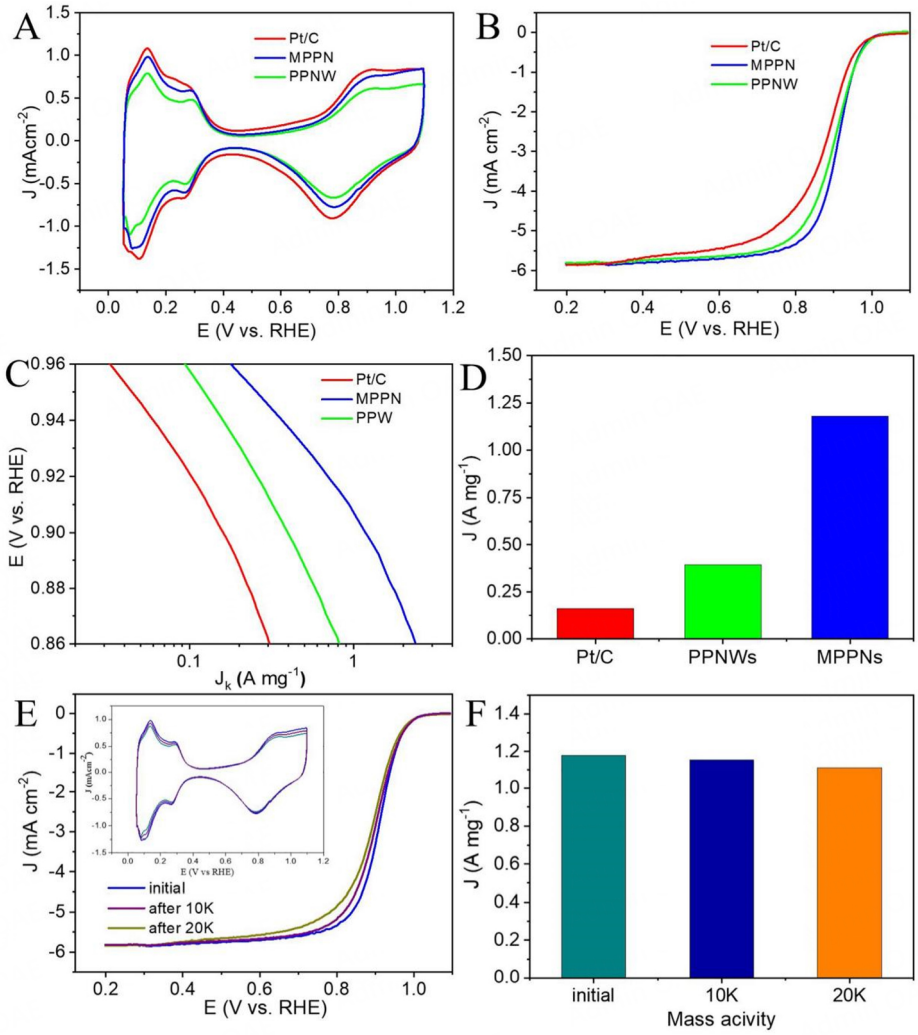

Figure 4. (A) CV curves of commercial TKK-Pt/C, MPPNs and PPNWs, recorded at 25 °C in an N_2-purged 0.1 M $HClO_4$ solution at 50 mV s^{-1}. (B) ORR polarization curves. (C) Mass activity (MA) Tafel slope and (D) histogram of mass activities at 0.9 V *vs.* RHE for Pt/C, MPPNs and PPNWs; (E) The ORR polarization curves of MPPNs after the durability test. (F) The mass activities of MPPNs at 0.9 V *vs.* RHE.

catalysts, demonstrates an improvement in the ORR kinetics. The mass activity of the catalysts was also analyzed at 0.9 V *vs.* RHE. As expected, the MPPNs exhibit the highest mass activity of 1.18 A mg^{-1}_{Pt+Pd}, significantly higher than that of PPNWs (0.395 A mg^{-1}_{Pt+Pd}) and Pt/C catalyst (0.16 A mg^{-1}_{Pt+Pd}), being approximately 7.4 times more active than commercial Pt/C catalyst [Figure 4D].

The electrochemical durability of the catalysts was further assessed by using the ADT. Figure 4E and F, Supplementary Figure 3 display the ORR polarization curves of MPPNs, PPNWs, and Pt/C after the ADT for 10 and 20 k cycles. The mass activity of the MPPNs demonstrated minimal change, decreasing by 6.91% and 25.5% after 10 and 20 k cycles of ADTs, respectively. In contrast, after cycling for 10 k, the mass activity of Pt/C and PPNW catalysts decreased by 40.3% and 47.3%, respectively. The results strongly suggest that MPPNs exhibit enhanced durability in ORR applications. The enhanced durability of MPPNs is likely attributed to their unique 1D mesoporous structure, which renders them less susceptible to dissolution, Ostwald ripening, and aggregation compared to nanoparticles during durability tests.

The electrocatalytic OER activities of MPPNs, PPNWs, and Pt/C catalysts were investigated in the mixed solution of 0.1 M $HClO_4$ and 1M ethanol. The CVs for the catalysts are shown in Figure 5A, displaying a typical oxidation profile with two characteristic oxidation peaks. During the forward scan, as the potential increases, ethanol oxidation generates currents, leading to a prominent anodic peak. Among the catalysts, the MPPNs exhibit the highest mass activity of 1.0 A mg^{-1}_{Pt+Pd}, 1.7 and 2.4 times larger than that of PPNWs (0.60 A mg^{-1}_{Pt+Pd}) and commercial Pt/C (0.33 A mg^{-1}_{Pt+Pd}), respectively. After 1 k cycles, the peak current density of MPPNs is 22.3 mA cm^{-2}, maintaining 93.1% of its initial values [Figure 5B]. The peak current density of MPPNs remains 84.5% of the initial values after the 2 K scan cycles, suggesting excellent stability of the MPPNs toward ethanol electrooxidation reaction.

The electrochemical stabilities of the catalysts toward ethanol electrooxidation reaction were further investigated by chronoamperometric (CA) experiments at 0.7 V in the mixed solution of 0.1 M $HClO_4$ and 1M ethanol. As demonstrated in Figure 5C, the CA curves reveal a rapid current decay on the commercial Pt/C electrodes due to the poisoning effect of the intermediate species absorbed on active site during the ethanol electrooxidation reaction. Conversely, the MPPNs exhibit a significantly slower current decay, indicating a superior CO tolerance. Upon completion of the test, the MPPNs displayed significantly higher oxidation currents than the Pt/C electrode. Figure 5D depicts the CO stripping voltammograms of both MPPNs and Pt/C. The onset potential of CO electrooxidation on MPPNs is about 0.2 V lower than that of Pt/C; the peak potential of MPPNs (0.54 V) is also negative by 50 mV compared to that of Pt/C (0.59 V). This suggests a remarkable enhancement in CO oxidation kinetics on MPPNs. The ratio of the forward and reverse peak current (Ip/Ir) for MPPNs is ~1.1, much higher than that of the Pt/C catalyst (0.90), indicating that the MPPN catalyst has better CO tolerance during EOR.

Working mechanism

As can be seen from the HRTEM images and the schematics of the crystal structure of the mesopores, MPPNs possess substantial active edge sites that contain certain atomic steps and high-index facets. Such edge sites should play a significant role in promoting electrocatalytic kinetics[41-43]. In addition, mass transfer is another important factor for the ethanol oxidation reaction. The hierarchical nanoporous structure of the MPPNs can allow for much more efficient mass diffusion, and the oxidative removal of intermediate species on Pt sites can be accelerated by the active oxygen-containing species such as -OH_{ads} and -O_{ads}[44]. The experimental results demonstrate the fascinating characteristics of MPPNs in catalyzing ethanol oxidation, such as high activity, excellent stability and exceptional resistance to CO poisoning.

To further reveal the role of edge sites in electrooxidation of ethanol on MPPNs, DFT calculations were conducted. According to TEM observation, the mesopore of MPPNs primarily consists of (111) and (200) crystal facets [Supplementary Figure 4]. Hence, three atomic structure models, PtPd(111), Pt(111)/(200) and PtPd(111)/(200), were constructed to assess the effects of the surface structure and composition on ethanol oxidation [Supplementary Figure 5]. Figure 6A-C displays their charge density distributions. It can be seen that the charges of Pt atoms on the edge sites of PtPt(111)/(200) are significantly higher than those of PtPd(111) and Pt(111)/(200), indicating that the edge sites of the mesopore enhance the charge density of catalyst surface. An increase in charge density of the catalyst surface should influence its catalytic performance[45-47]. To further explore the effect of charge change, the electronic characteristics of *d* orbitals are calculated to analyze the catalytic activity. Figure 6D-F shows the partial density of states (PDOS) of PtPd(111), Pt(111)/(200) and PtPd(111)/(200), respectively. The *d*-states of PtPd(111) are relatively discrete, resulting in the *d*-band center (ε_d = -2.08 eV) far away from the Fermi level. The *d* states of PtPd(111)/(200) are more enriched near the Fermi level with ε_d of -1.91 eV, and the *d*-band center of PtPd(111)/(200) is closer to the Fermi level than of Pt(111)/(200) (ε_d = -2.03 eV), suggesting that the active edge sites of PtPd(111)/(200) are beneficial for the catalytic activity.

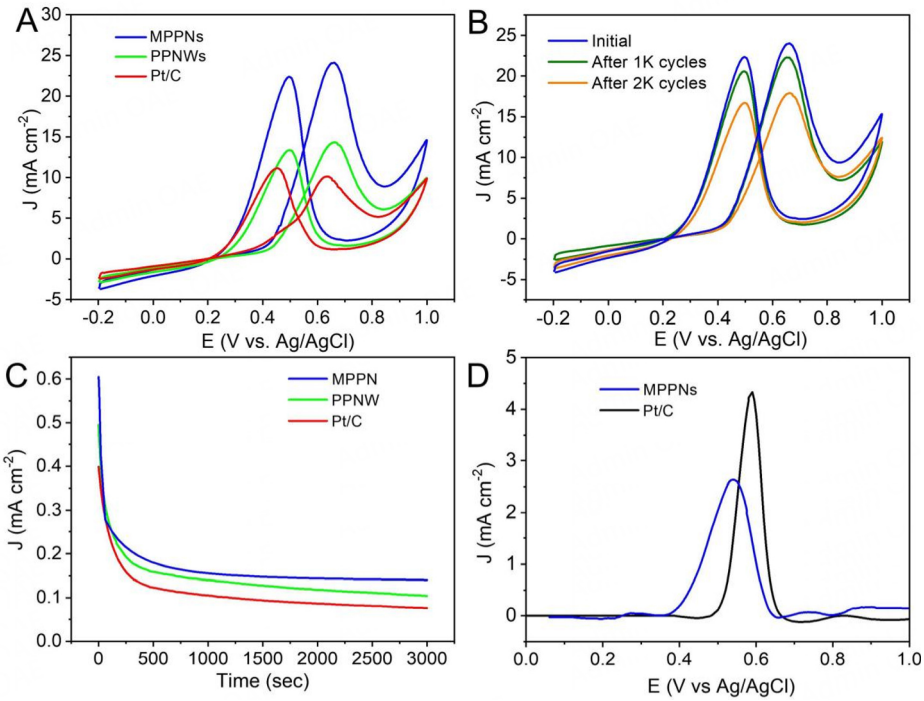

Figure 5. (A) CV curves obtained on commercial TKK-Pt/C, MPPNs and PPNWs in 0.1 M $HClO_4$ + 1M ethanol aqueous solution. (B) CV curves obtained on PPNWs after a durability test. (C) Chronoamperometric curves obtained on commercial TKK-Pt/C, MPPNs and PPNWs. (D) CO stripping voltammograms of Pt/C and MPPNs.

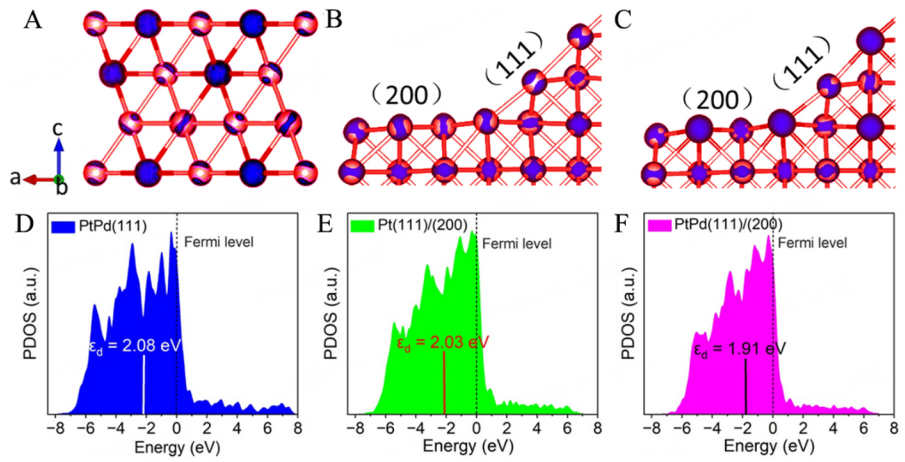

Figure 6. (A-C) Charge density of PtPd(111), Pt(111)(200) and PtPd(111)(200) with isosurface level of 0.315 *e* $bohr^{-3}$. The blue regions represent charge accumulation. (D-F) PDOS of PtPd(111), Pt(111)/(200) and PtPd(111)/(200).

Figure 7A and Supplementary Figure 6 display the energy profile of ethanol adsorption. The adsorption energies (E_a) for all adsorption sites on PtPd(111) are negative, with the lowest E_a being -0.22 eV. This indicates that ethanol can stably adsorb on the PtPd(111) surface based on thermodynamic consideration, and the adsorption process is exothermic. On Pt(111)/(200), a positive E_a value is observed for some sites on both the (111) and (200) facets, implying that the adsorption process is endothermic and the ethanol cannot stably adsorb at these sites. In addition, the E_a of ethanol adsorbed on the (111) facet (-0.28 eV) is lower than that of the (200) surface (-0.26 eV), indicating that the (111) facet is more favorable for ethanol adsorption.

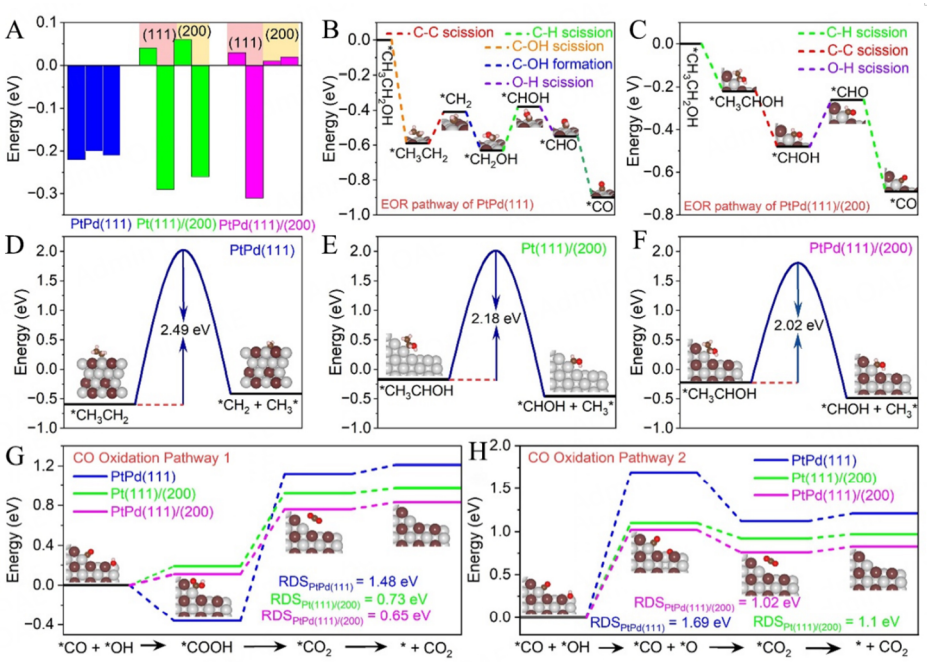

Figure 7. (A) Ethanol adsorption energy at different sites. (B and C) The schematic representations and calculated reaction pathways for ethanol decomposition on the surface of PtPd(111), and PtPd(111)/(200), respectively. (D-F) The energy barriers of breaking C-C bond on PtPd(111), Pt(111)/(200) and PtPd(111)/(200), respectively. (G and H) The schematic representations and calculated reaction pathways for CO oxidation.

The E_a values of edge sites of PtPd(111)/(200) suggest the ethanol preferential adsorption on the (111) facet. The above calculation results reveal that the mesopores composed of (111)/(200) edge sites may offer localized reduction sites in ethanol adsorption on the catalyst surface. Furthermore, compared with PtPd(111) and Pt(111)/(200), the PtPd(111)/(200) exhibits lower ethanol E_a, which may be beneficial for enhancing selectivity and suppressing other competitive reactions. The low ethanol E_a of PtPd(111)/(200) can be attributed to its *d*-orbital electronic properties, where the closer the *d*-band center is to the Fermi level, the easier it is for electron transfer from *d* orbitals to the adsorbed ethanol, thus making the ethanol adsorbed more strongly[48].

The energy variation and energy barrier of the EOR process on PtPd(111), PtPd(111)/(200) and Pt(111)/(200) are shown in Figure 7B and C, Supplementary Figures 7-9. The calculation results show that the initial decomposition process on PtPd(111) prefers C-OH scission rather than C-H or O-H scission, resulting in the formation of $^*CH_3CH_2$. $^*CH_3CH_2$ dehydrogenations to form $^*CH_2CH_2$ or $^*CH_3CH$ requires overcoming energy barriers of 2.68 and 2.72 eV, much higher than that of C-C scission (2.49 eV). Thus, C-C scission is preferred over C-H scission. Similarly, the $^*CH_2$ intermediate is more inclined to combine with OH^- to form $^*CH_2OH$, and then undergoes C-H scission, O-H scission and C-H scission, until $^*CO$ intermediate is formed. PtPd(111)/(200) has a similar EOR pathway as Pt(111)/(200), suggesting that the addition of Pd does not influence the reaction pathway. During the initial decomposition process on PtPd(111)/(200), both $^*CH_3CHOH$ and $^*CH_3CH_2$ intermediates may be formed. However, the energy barrier of C-H scission (2.14 eV) is lower than that of C-OH scission (2.30 eV); thus, $^*CH_3CHOH$ is generated preferentially. Then, C-C scission is preferred during the following decomposition process, and the *CHOH intermediate undergoes O-H and C-H scission to form *CO. Figure 7D-F displays the energy barriers of PtPd(111), Pt(111)/(200), and PtPd(111)/(200) for C-C scission, and PtPd(111)/(200) exhibits the lowest energy barrier (2.02 eV). The above calculation results confirm that the mesoporous structure can simplify the ethanol

oxidation process, while the introduction of Pd can reduce reaction energy barriers; thus, MPPNs deliver outstanding catalytic performance on ethanol electrooxidation.

CO_{ads} is the main poisoning species under an acidic environment. The high electrocatalytic activity and stability indicate that MPPNs are more tolerant toward CO poisoning than commercial Pt/C catalysts. Supplementary Figure 10 displays the binding energies of CO adsorbed on the catalyst surface, where the binding energies of PtPd(111), Pt(111)/(200), and PtPd(111)/(200) are 1.97, 1.91 and 1.78 eV, respectively. The calculation results further confirm that PtPd(111)/(200) has the weakest adsorption strength for CO. To understand the CO oxidation, theoretic calculations have been conducted using DFT. Key oxidant species, including OH and O, are introduced onto the catalyst surface. CO elimination occurs via coupling with adsorbed OH or O. DFT calculations reveal that the (100) surfaces of Pt(111)/(200) and PtPd(111)/(200) possess superior adsorption capacity for OH compared to their (111) surfaces [Supplementary Figure 11]. Therefore, atomic models were constructed with CO adsorbed on (111) and OH adsorbed on (200) surfaces to assess CO elimination capacity. Figure 7G and H illustrates the energy changes associated with elementary steps over PtPd(111), Pt(111)/(200) and PtPd(111)/(200). On the PtPd(111) facet, the coupling of *CO and *OH (*CO + *OH → *COOH) is exothermic (-0.36 eV), while the conversion of $^*OH \rightarrow {}^*O$ is endothermic (1.69 eV), indicating that the coupling with adsorbed OH is the primary mechanism for CO removal from the catalyst surface. The subsequent dehydrogenation (*COOH → *COO + $H^+ + e^-$) is the rate-determining step (RDS) with an energy barrier of 1.48 eV. On the edge sites of Pt(111)/(200) and PtPd(111)/(200) surfaces, the coupling with adsorbed OH and dehydrogenation of $^*OH$ are endothermic processes, suggesting that $^*OH$ and $^*O$ can coexist and potentially act as oxidation agents simultaneously. The maximum input energies for CO oxidation on PtPd(111), Pt(111)/(100) and PtPd(111)/(100) are 1.48, 1.1 and 1.02 eV, respectively. These calculation results reveal that constructing the mesoporous structure can influence the oxidation pathway of CO, whereas the incorporation of Pd can decrease the energy required for CO oxidation.

CONCLUSION

In summary, we have successfully prepared MPPNs with highly ordered mesostructure and precisely controlled size and morphology. The MPPNs exhibit excellent bifunctional electrocatalytic activity toward both oxygen reduction and ethanol oxidation. Moreover, the catalysts exhibit superior stability and CO-tolerance. DFT studies confirm the critical role of the synergistic effect of neighboring (111) and (200) facets on the edge sites. The mesoporous structure regulates the active sites, and affects the oxidation pathway of ethanol and CO, enhancing the electrocatalytic activity and stability. This work provides an effective strategy for precisely fabricating metallic mesostructures and developing high-performance catalysts for direct alcohol fuel cells and beyond.

DECLARATIONS

Authors' contributions

Writing, investigation, methodology: Wang, S.; Zhao, Z.
Supervision, writing: Hu, Y.
Conceptualization, supervision, writing: Jiang, S.; Zhang, X.

Availability of data and materials

More data on our findings can be found in the Supplementary Material.

Financial support and sponsorship
This work was supported by the Scientific Technological Innovation Program of Hubei Province and the National Natural Science Foundation of China (21972027).

Conflicts of interest
All authors declared that there are no conflicts of interest.

Ethical approval and consent to participate
Not applicable.

Consent for publication
Not applicable.

REFERENCES
1. Chang, J.; Wang, G.; Li, C.; et al. Rational design of septenary high-entropy alloy for direct ethanol fuel cells. *Joule* **2023**, *7*, 587-602. DOI
2. Fuku, X.; Modibedi, M. Performance of $BiCu_2O$ modified Pd/C as an anode electrocatalyst for direct ethanol fuel cell system. *Catal. Today.* **2024**, *425*, 114305. DOI
3. Fajardo, S.; Ocón, P.; Rodríguez, J.; Pastor, E. Co supported on N and S dual-doped reduced graphene oxide as highly active oxygen-reduction catalyst for direct ethanol fuel cells. *Chem. Eng. J.* **2023**, *461*, 142053. DOI
4. Ao, W.; Ren, H.; Cheng, C.; et al. Mesoporous PtPb nanosheets as efficient electrocatalysts for hydrogen evolution and ethanol oxidation. *Angew. Chem. Int. Ed.* **2023**, *62*, e202305158. DOI
5. Xiao, L.; Li, G.; Yang, Z.; et al. Engineering of amorphous PtO_x interface on Pt/WO_3 nanosheets for ethanol oxidation electrocatalysis. *Adv. Funct. Mater.* **2021**, *31*, 2100982. DOI
6. Yoon, Y. S.; Basumatary, P.; Kilic, M. E.; et al. Novel GaPtMnP alloy based anodic electrocatalyst with excellent catalytic features for direct ethanol fuel cells. *Adv. Funct. Mater.* **2022**, *32*, 2111272. DOI
7. Wang, Z.; Tang, Y.; Liu, S.; et al. Energy transfer-mediated multiphoton synergistic excitation for selective C(*sp3*)-H functionalization with coordination polymer. *Nat. Commun.* **2024**, *15*, 8813. DOI PubMed PMC
8. Zhang, Y.; Liu, X.; Liu, T.; et al. Rhombohedral Pd-Sb nanoplates with Pd-terminated surface: an efficient bifunctional fuel-cell catalyst. *Adv. Mater.* **2022**, *34*, e2202333. DOI
9. Wang, H.; Abruña, H. D. Adsorbed enolate as the precursor for the C-C bond splitting during ethanol electrooxidation on Pt. *J. Am. Chem. Soc.* **2023**, *145*, 6330-8. DOI
10. Sun, B.; Zhong, W.; Ai, X.; Zhang, C.; Li, F.; Chen, Y. Engineering low-coordination atoms on RhPt bimetallene for 12-electron ethanol electrooxidation. *Energy. Environ. Sci.* **2024**, *17*, 2219-27. DOI
11. Kim, K. H.; Hobold, G. M.; Steinberg, K. J.; Gallant, B. M. Confinement effects of hollow structured Pt-Rh electrocatalysts toward complete ethanol electrooxidation. *ACS. Nano.* **2023**, *17*, 14176-88. DOI PubMed
12. Han, C.; Lyu, Y.; Wang, S.; et al. Noncovalent interactions on the electrocatalytic oxidation of ethanol on a Pt/C electrocatalyst. *Carbon. Energy.* **2023**, *5*, e339. DOI
13. Liang, C.; Zhao, R.; Chen, T.; et al. Recent approaches for cleaving the C-C bond during ethanol electro-oxidation reaction. *Adv. Sci.* **2024**, *11*, e2308958. DOI PubMed PMC
14. Peng, K.; Liu, L.; Bhuvanendran, N.; Lee, S. Y.; Xu, Q.; Su, H. Efficient one-dimensional Pt-based nanostructures for methanol oxidation reaction: an overview. *Int. J. Hydrogen. Energy.* **2023**, *48*, 29497-517. DOI
15. Yu, R.; Shao, R.; Ning, F.; et al. Electronic and geometric effects endow PtRh jagged nanowires with superior ethanol oxidation catalysis. *Small* **2024**, *20*, e2305817. DOI
16. Wang, Q.; Zhu, R.; Deng, P.; et al. Rhodium decorated stable platinum nickel nanowires for effective ethanol oxidation reaction. *Sci. China. Mater.* **2023**, *66*, 679-85. DOI
17. Gao, L.; Sun, T.; Chen, X.; et al. Identifying the distinct roles of dual dopants in stabilizing the platinum-nickel nanowire catalyst for durable fuel cell. *Nat. Commun.* **2024**, *15*, 508. DOI PubMed PMC
18. Zhao, X.; Takao, S.; Yoshida, Y.; et al. Roles of structural defects in polycrystalline platinum nanowires for enhanced oxygen reduction activity. *Appl. Catal. B. Environ.* **2023**, *324*, 122268. DOI
19. Zhou, Z.; Zhang, H.; Feng, X.; Ma, Z.; Ma, Z.; Xue, Y. Progress of Pt and iron-group transition metal alloy catalysts with high ORR activity for PEMFCs. *J. Electroanalytical. Chem.* **2024**, *959*, 118165. DOI

20. Liu, X.; Zhao, Z.; Liang, J.; et al. Inducing covalent atomic interaction in intermetallic Pt alloy nanocatalysts for high-performance fuel cells. *Angew. Chem. Int. Ed.* **2023**, *62*, e202302134. DOI
21. Xia, T.; Zhao, K.; Zhu, Y.; et al. Mixed-dimensional Pt-Ni alloy polyhedral nanochains as bifunctional electrocatalysts for direct methanol fuel cells. *Adv. Mater.* **2023**, *35*, e2206508. DOI
22. Nie, M.; Xu, Z.; Luo, L.; Wang, Y.; Gan, W.; Yuan, Q. One-pot synthesis of ultrafine trimetallic PtPdCu alloy nanoparticles decorated on carbon nanotubes for bifunctional catalysis of ethanol oxidation and oxygen reduction. *J. Colloid. Interface. Sci.* **2023**, *643*, 26-37. DOI
23. Liu, Y.; Sheng, S.; Wu, M.; et al. Controllable synthesis of PtIrCu ternary alloy ultrathin nanowires for enhanced ethanol electrooxidation. *ACS. Appl. Mater. Interfaces.* **2023**, *15*, 3934-40. DOI
24. Carvalho, L. L.; Tanaka, A. A.; Colmati, F. Palladium-platinum electrocatalysts for the ethanol oxidation reaction: comparison of electrochemical activities in acid and alkaline media. *J. Solid. State. Electrochem.* **2018**, *22*, 1471-81. DOI
25. Qian, K.; Hao, F.; Wei, S.; et al. Synthesis of well-dispersed Pt-Pd nanoparticles stabilized by silsesquioxanes with enhanced catalytic activity for formic acid electrooxidation. *J. Solid. State. Electrochem.* **2017**, *21*, 297-304. DOI
26. Luo, W.; Zhou, H.; Fu, C.; Huang, Z.; Gao, N.; Kuang, Y. Preparation and characterization of porous sponge-like Pd@Pt nanotubes with high catalytic activity for ethanol oxidation. *Mater. Lett.* **2016**, *173*, 43-6. DOI
27. Zhang, Y.; Shu, G.; Shang, Z.; et al. Electronic and coordination effect of PtPd nanoflower alloys for the methanol electrooxidation reaction. *ACS. Sustain. Chem. Eng.* **2023**, *11*, 8958-67. DOI
28. Li, B.; Zhang, H.; Kaelin, J.; et al. Carbon-supported and shape-controlled PtPd nanocrystal synthesis in flowing deep eutectic solvents for the methanol oxidation reaction. *ACS. Appl. Nano. Mater.* **2023**, *6*, 3184-90. DOI
29. Ding, K.; Wang, Y.; Yang, H.; et al. Electrocatalytic activity of multi-walled carbon nanotubes-supported Pt_xPd_y catalysts prepared by a pyrolysis process toward ethanol oxidation reaction. *Electrochim. Acta.* **2013**, *100*, 147-56. DOI
30. Perdew, J. P.; Burke, K.; Ernzerhof, M. Generalized gradient approximation made simple. *Phys. Rev. Lett.* **1996**, *77*, 3865-8. DOI PubMed
31. Blöchl, P. E. Projector augmented-wave method. *Phys. Rev. B. Condens. Matter.* **1994**, *50*, 17953-79. DOI PubMed
32. Lee, Y.; Ko, A.; Kim, D.; Han, S.; Park, K. Octahedral Pt-Pd alloy catalysts with enhanced oxygen reduction activity and stability in proton exchange membrane fuel cells. *RSC. Adv.* **2012**, *2*, 1119-25. DOI
33. Bai, Z.; Luo, J.; Ming, D.; Wang, C.; Xu, H.; Ye, W. High active and durable N-doped carbon spheres-supported flowerlike PtPd nanoparticles for electrochemical oxidation of liquid alcohols. *Electrochim. Acta.* **2020**, *356*, 136794. DOI
34. Ying, J.; Xiao, Y.; Chen, J.; et al. Fractal design of hierarchical PtPd with enhanced exposed surface atoms for highly catalytic activity and stability. *Nano. Lett.* **2023**, *23*, 7371-8. DOI
35. Cheng, Y.; Shen, P. K.; Saunders, M.; Jiang, S. P. Core-shell structured $PtRuCo_x$ nanoparticles on carbon nanotubes as highly active and durable electrocatalysts for direct methanol fuel cells. *Electrochim. Acta.* **2015**, *177*, 217-26. DOI
36. Shao, C.; Cui, Y.; Zhang, L.; et al. Boosting propane purification on $Pt/ZrOSO_4$ nanoflowers: insight into the roles of different sulfate species in synergy with Pt. *Sep. Purif. Technol.* **2023**, *304*, 122367. DOI
37. Ho, V. T.; Pan, C. J.; Rick, J.; Su, W. N.; Hwang, B. J. Nanostructured $Ti_{0.7}Mo_{0.3}O_2$ support enhances electron transfer to Pt: high-performance catalyst for oxygen reduction reaction. *J. Am. Chem. Soc.* **2011**, *133*, 11716-24. DOI
38. Ando, F.; Gunji, T.; Tanabe, T.; et al. Enhancement of the oxygen reduction reaction activity of pt by tuning Its *d*-band center via transition metal oxide support interactions. *ACS. Catal.* **2021**, *11*, 9317-32. DOI
39. Li, J.; Chen, Y.; Bai, R.; et al. Construction of Pd/Ni_2P-Ni foam nanosheet array electrode by in-situ phosphatization-electrodeposition strategy for synergistic electrocatalytic hydrodechlorination. *Chem. Eng. J.* **2022**, *435*, 134932. DOI
40. Chen, H.; Shuang, H.; Lin, W.; et al. Tuning interfacial electronic properties of palladium oxide on vacancy-abundant carbon nitride for low-temperature dehydrogenation. *ACS. Catal.* **2021**, *11*, 6193-9. DOI
41. Tian, N.; Zhou, Z. Y.; Sun, S. G.; Ding, Y.; Wang, Z. L. Synthesis of tetrahexahedral platinum nanocrystals with high-index facets and high electro-oxidation activity. *Science* **2007**, *316*, 732-5. DOI
42. Xu, X.; Zhang, X.; Sun, H.; et al. Synthesis of Pt-Ni alloy nanocrystals with high-index facets and enhanced electrocatalytic properties. *Angew. Chem. Int. Ed.* **2014**, *53*, 12522-7. DOI
43. Zhao, Z. L.; Wang, Q.; Du, H.; Liang, T.; An, H. M.; Li, C. M. Sub-15 nm Pd@PtCu concave octahedron with enriched atomic steps as enhanced oxygen reduction electrocatalyst. *J. Power. Sources.* **2019**, *434*, 226742. DOI
44. Hu, S.; Li, X.; Ali, A.; Zhang, X.; Kang, S. P. Large-scale synthesis of porous Pt nanospheres/three-dimensional graphene hybrid materials as a highly active and stable electrocatalyst for oxygen reduction reaction. *ChemistrySelect* **2021**, *6*, 2080-4. DOI
45. Wang, M.; Liu, X.; Wu, X. Realizing efficient electrochemical overall water electrolysis through hierarchical CoP@NiCo-LDH nanohybrids. *Nano. Energy.* **2023**, *114*, 108681. DOI
46. Yang, Y.; Wang, Y.; He, H. L.; et al. Covalently connected $Nb_4N_{5-x}O_x$-MoS_2 heterocatalysts with desired electron density to boost hydrogen evolution. *ACS. Nano.* **2020**, *14*, 4925-37. DOI
47. He, D.; Song, X.; Li, W.; et al. Active electron density modulation of Co_3O_4-based catalysts enhances their oxygen evolution performance. *Angew. Chem. Int. Ed.* **2020**, *59*, 6929-35. DOI
48. Luo, S.; Zhang, L.; Liao, Y.; et al. A tensile-strained Pt-Rh single-atom alloy remarkably boosts ethanol oxidation. *Adv. Mater.* **2021**, *33*, e2008508. DOI